Influence of Electron−Hole Pair Excitation on Dissociative Sticking

Signe Kvist Mengel and Gert D. Billing*

Department of Chemistry, H. C. Ørsted Institute, University of Copenhagen, 2100 Copenhagen Ø, Denmark

Received: June 24, 1997; In Final Form: October 1, 1997[⊗]

Using a semiclassical model that treats the phonons and electrons of a metal quantally within a second quantization formalism and the dynamics of the incoming molecule classically, we have calculated the dissociative sticking and energy accommodation as a function of band structure for the electron−hole pair excitation. It is shown that the electronic band structure has some influence on the reactivity, such that the inclusion of this aspect makes the 111 surface more reactive than the 100 surface—in agreement with experimental findings.

1. Introduction

Recent progress in ab initio density functional calculations on molecule surface interaction[1] has made a number of data on the lowest adiabatic potential energy surface available. The ab initio data give information on the potential barrier and molecular geometries at a number of selected approach sites and angles. Usually up to a maximum of a few hundred points have been calculated. Often these points are represented by a potential surface in two dimensions $V(r,z)$ where r is the bond distance of the diatomic molecule and z the distance from the center of mass to the surface. However, the full dynamical problem involves six degrees of freedom for the molecule and $3N_\alpha - 6$ for the solid consisting of N_α atoms. Even for light molecules as hydrogen the phonon excitation may also not be neglected a priori.[2,3] Previous investigations have shown that also electron-hole pair excitation can be important,[4] i.e., the assumption that the dynamical process takes place on an adiabatic potential energy surface breaks down. These nonadiabatic processes will give additional friction and enhance the residence lifetime of the molecule at the surface; i.e., coupling of the various degrees of freedom is enhanced and even the phonon-coupling increases.

Thus the complete understanding of chemisorption processes involves the solution of a many-body problem in the phonons and electrons of the system. This also requires a construction of potential surface functions that include these aspects. We have in a number of previous papers formulated a semiclassical theory[3,5−7] that is capable of including these aspects. The theory is briefly reviewed below. The present paper improves the description of the one-electron wave functions used for describing the electron−hole pair excitation. Here 2D-wave functions are introduced and a five-band model for the band structure is used. Results are compared with the previous obtained using 1D-wave functions and a two-band model and with calculations which neglect electron−hole pair excitation altogether. The system chosen for investigation is the hydrogen−copper system for which a multidimensional embedded diatomics in molecules (EDIM) potential has recently been constructed[3] by fitting the parameters to ab initio density functional data from.[8]

2. Theory

The semiclassical theory which has been developed in our previous publications[3−5] treats the phonons and electrons within a quantum description using a second quantization approach.

The motion of the incoming atom/molecule is solved simultaneously with the excitation processes in a self-consistent manner. Hence the motion is governed by an effective potential

$$H_{\text{eff}} = \frac{1}{2M}(P_X^2 + P_Y^2 + P_Z^2) + \frac{1}{2m}(p_x^2 + p_y^2 + p_z^2) + V_0(\mathbf{R}, \mathbf{r}) + V_{\text{eff}}^{\text{ph}} + V_{\text{eff}}^{\text{elho}} + E_{\text{int}} \quad (1)$$

where M is the mass and m the reduced mass of the diatom, P_X, P_Y, P_Z are the momenta connected to the motion of the center of mass of the diatom and p_x, p_y, p_z the momenta for the internal degrees of freedom (rotation and vibration). The interaction potential is expanded around the equilibrium position for the metal atoms. The first term in this expansion is V_0. The next terms (usually only the linear term is included) are represented by $V_{\text{eff}}^{\text{ph}}$ − an effective potential

$$V_{\text{eff}}^{\text{ph}} = \sum_k V_k^{(1)} \langle \Phi_{\text{ph}}(t) | Q_k | \Phi_{\text{ph}}(t) \rangle \quad (2)$$

where the expectation value of the phonon coordinates Q_k is taken. $V_k^{(1)}$ is the first derivative of the interaction potential with respect to phonon mode Q_k and $\Phi_{\text{ph}}(t)$ the wavefunction for the phonons. Thus the phonons are excited during collision—thereby changing the wavefunction and in turn the effective potential governing the motion. Other excitation processes are those due to electron−hole pair excitation. It is possible[3,4] to formulate the response from this excitation in a way that gives yet an additional effective potential $V_{\text{eff}}^{\text{elho}}$ governing the dynamics of the molecule. Finally E_{int} is the energy transferred to the metal—it can be divided into energy transfer to the phonons and electrons. The effective potential which arises due to the coupling of the motion of the molecule and the electrons of the metal is

$$V_{\text{eff}}^{\text{elho}} = \langle \Psi_{\text{el}}(t) | U_C | \Psi_{\text{el}}(t) \rangle \quad (3)$$

where U_C is the screened Coulomb potential (see section 5) and $\Psi_{\text{el}}(t)$ the wavefunction for the electrons. We have previously given an approximate solution of the electronic excitation problem using a second-quantization approach.[4] This theory resulted in an effective potential of the form

[⊗] Abstract published in *Advance ACS Abstracts,* November 15, 1997.

S1089-5647(97)02061-0 CCC: $14.00

$$V_{\text{eff}}^{\text{elho}} = 2Re \sum_{i,\epsilon_i<\epsilon_F} \sum_{j,\epsilon_j>\epsilon_F} j_0(2\sqrt{A_{ii}^{(2)}}) \frac{U_{ij}}{\hbar} \int_{t_0}^{t} U_{ij}^{*} \sin(\omega_{ji}(t-t'))\, dt' \quad (4)$$

where the matrix elements U_{ij} are given by

$$U_{ij} = \langle i\,|U_C|j\rangle \quad (5)$$

j_0 is a Bessel function, $\omega_{ji} = (\epsilon_j - \epsilon_i)/\hbar$, and $A_{ii}^{(2)} = \sum_j |A_{ij}^{(1)}|^2$ where

$$A_{ij}^{(1)} = \frac{1}{\hbar} \int_{t_0}^{t} U_{ij}(t) \exp(i\omega_{ij}t')\, dt' \quad (6)$$

We have introduced the one-electron wave functions i and the Fermi-energy ϵ_F. The Fermi energy is taken as that of a "free" electron. However, for the 2-D calculations we make the restriction that the electron is constrained to move in two dimensions. The density of states is determined by how much space (ΔA) the states occupy in reciprocal space. Having N electrons inside the area A gives $\Delta A = (2\pi)^2/A$. Introducing the density of states N/A we get the Fermi vector from the equation

$$N = 2\frac{\pi {k_F}^2}{\Delta A} \quad (7)$$

Assuming that each copper atom donates one electron to the electron gas gives altogether two electrons per unit cell d^2 and hence the density $2/d^2$ and a Fermi vector $k_F = 0.982$ Å^{-1}. Thus the Fermi energy 3.545ϵ ($1\ \epsilon = 100$ kJ/mol) lies in the lower band (see Figures 2−4). When performing the summation over states below the Fermi level we introduce a finite grid in k_x, k_y space and use

$$\sum_{\mathbf{k}} \rightarrow \sum_{k_x} \sum_{k_y} \frac{\Delta k_x \Delta k_y}{\Delta A} \quad (8)$$

We have used the same density for the both the 100 and the 111 surface, i.e., any difference seen between these two surfaces does not come from a difference in the density of states but rather from their "symmetry" in direct as well as momentum space.

The "transition" matrix elements U_{ij} will depend upon time through the time-dependence of the trajectory and the summation in eq 4 is over states i with energy less than the Fermi energy and states j with energy above the Fermi energy. In section 4 we discuss how the one-electron wavefunctions are determined.

3. The Potential

To include phonon and electron excitation processes, the potential must depend on the normal mode coordinates for the metal and the electron coordinates of the electrons. This is acheived using an EDIM (embedded diatomics in molecules) potential[9] and by assuming that the excess charge on the incoming molecule—a charge arising from charge transfer from the metal to the molecule—interacts with the electrons in the metal through a screened Coulomb potential. The charge transfer process is an inherent part of the adiabatic (electronically relaxed) ab initio data for the interaction. However, in order to simulate the experimental situation we should account for the fact that the collision process may not take place on the adiabatic surface—but rather on a "diabatic" surface which includes electronic friction arising from nonadiabatic processes.

The construction of the EDIM potential is based upon a combination of the DIM method for constructing potentials for polyatomic systems from diatomic fragment potentials and the EAM (embedded atom) method for interaction of an atom with the electron gas of the metal. The EDIM potential contains a number of parameters, which are determined by fitting those to available ab initio DFT (density functional) calculations. The screened Coulomb potential is an often used model for the interaction of a charged particle with a medium consisting of electrons distributed on an "ionic" background. Thus both models are reasonable from a physical point of view and the approximations quite transparent. Furthermore realistical molecular dynamical calculations can be carried out using these two models.

The construction of the EDIM potential has been given in detail in a previous publication[3] and will therefore only be briefly reviewed here. The lowest adiabatic surface is obtained by solving a 2×2 secular equation, i.e.

$$W_{11} = {}^1/_6(H_{11} + H_{22} + H_{12}) - {}^1/_6\sqrt{H_{11}^2 + H_{22}^2 - H_{11}H_{22} + 2H_{12}(2H_{12} + H_{11} + H_{22})} \quad (9)$$

where the matrix elements H_{ij} are expressed in terms of Coulomb and exchange integrals

$$H_{11} = 4(Q_{ab} + Q_{aM} + Q_{bM} + J_{ab}) - 2(J_{aM} + J_{bM}) \quad (10)$$

$$H_{22} = 4(Q_{ab} + Q_{aM} + Q_{bM} + J_{aM} + J_{bM}) - 2J_{ab} \quad (11)$$

$$H_{12} = -2(Q_{ab} + Q_{aM} + Q_{bM} + J_{ab} + J_{aM} + J_{bM}) \quad (12)$$

where a and b denote the two atoms and M the metal. The Coulomb and exchange integrals are represented as sums and differences of singlet and triplet curves

$$Q_{ab} = {}^1/_2(E_{ab}^s + E_{ab}^t) \quad (13)$$

$$J_{ab} = {}^1/_2(E_{ab}^s - E_{ab}^t) \quad (14)$$

For the gas molecule we use Morse and anti-Morse potential functions for the singlet and triplet curves respectively, but for the atom−metal interaction the embedded atom expressions

$$E_{aM}^s = F_a(\rho_a) + \sum_{\alpha=1}^{M} \phi_{a\alpha}(R_{a\alpha}) \quad (15)$$

$$E_{aM}^t = -F_a(\rho_a) + \sum_{\alpha=1}^{M} \phi_{a\alpha}(R_{a\alpha}) \quad (16)$$

are used. The first term is a contribution from an embedding energy $F_a(\rho)$, which is a function of the electron density created by the metal at atom a, and the second term consists of screened Coulomb pair potentials

$$\phi_{a\alpha}(R) = Z_a(R)\, Z_\alpha(R)/R \quad (17)$$

where Z_a and Z_α are effective nuclear charges

$$Z_a(R) = Z_{0a}(1 + \beta_a R^{\nu a}) \exp(-\alpha_a R) \quad (18)$$

The effective charge and the embedding function contain parameters that has been determined by fitting the energy W_{11} to available ab initio DFT calculations. The advantage of this analytical presentation is that the potential does depend upon

TABLE 1: An Overview of the Different One-Electron Potentials Investigated

1D-model	$U(x) = 2U_0 \cos(2\pi/d_{1D})x$
2D-model, Cu(100)	$U(\mathbf{r}) = 2U_0 \cos \mathbf{r}\cdot\mathbf{b}_1 + 2U_0 \cos \mathbf{r}\cdot\mathbf{b}_2$
2D-model, Cu(111)	$U(\mathbf{r}) = 2U_0 \cos \mathbf{r}\cdot\mathbf{b}_1 + 2U_0 \cos \mathbf{r}\cdot\mathbf{b}_2 + 2U_0 \cos \mathbf{r}\cdot(\mathbf{b}_1 + \mathbf{b}_2)$

the position of the metal atoms and hence also upon the normal mode coordinates for the phonons.

4. Band Structure

The evaluation of the effective potential $V_{\text{eff}}^{\text{elho}}$ requires that the band structure of the metal is known. This section describes the two different models of the band structure investigated.

4.1. One-Electron Potential. The one-electron wavefunctions ψ and the eigenenergies ψ are the solutions to the time-independent Schrödinger equation

$$\left(-\frac{\hbar^2}{2m_e}\nabla^2 + U\right)\psi = \epsilon\psi \tag{19}$$

where m_e is the electron mass. The effective potential U is the potential originating from the interaction of the electron and the positive ions of the lattice and from the interaction of the electron and the other electrons of the metal. U is assumed to have the symmetry of the crystal lattice of the metal. Because the potential U is periodic in the lattice it can be written as

$$U(\mathbf{r}) = \sum_{\mathbf{G}} U_{\mathbf{G}}\, e^{i\mathbf{G}\cdot\mathbf{r}} \tag{20}$$

where the sum runs over all reciprocal lattice vectors **G**.

Different models for the bandstructure are obtained by choosing different forms of the effective potential U. Previously Billing[4] used a potential that restricted the electrons to move in one dimension. The effective potential was assumed to be a simple periodic potential with a period d_{1D} equal to the nearest-neighbor distance of the atomic nuclei in the copper lattice (Table 1). We have used $d_{1D} = 2.56$ Å. In the following this model is referred to as the 1D-model.

We have extended the 1D-model so that the electrons instead of being constrained by the potential to move along a line are allowed to move in a plane. This new model is hereafter referred to as the 2D-model. As in the 1D-model we have used a simple expression for the one-electron potential U. But as the electrons are free to move in a plane it seems natural to demand that U has the periodicity of the atomic nuclei in the top layer of the crystal. Because of this requirement U depends in the 2D-model on the orientation of the crystal.

We have investigated two surfaces: a Cu(100) and a Cu(111) surface. Those surfaces are illustrated in Figure 1 and the expressions for the potentials are given in Table 1. The vectors $\boldsymbol{b}_1$ and $\boldsymbol{b}_2$ in Table 1 are the basis vectors of the reciprocal lattice. If the lattice constant of copper is denoted by d_{2D} and the orthonormal basis vectors of the plane are called **i** and **j** the basis vectors of the lattice are: $\mathbf{b}_1 = (2\pi/d_{2D})\mathbf{i} + (2\pi/d_{2D})\mathbf{j}$ and $\mathbf{b}_2 = (2\pi/d_{2D})\mathbf{i} - (2\pi/d_{2D})\mathbf{j}$ for Cu(100) and $\mathbf{b}_1 = \{(2\sqrt{2}\pi)/d_{2D}\}\mathbf{i} - \{(2\sqrt{2}\pi)/(\sqrt{3}d_{2D})\}\mathbf{j}$ and $\mathbf{b}_2 = \{(4\sqrt{2}\pi)/(\sqrt{3}d_{2D})\}\mathbf{j}$ for Cu(111), where $d_{2D} = 3.61$ Å.

4.2. The Approximative Solution. From elementary textbooks on solid state physics it is well-known that the one-electron eigenfunctions ψ and the corresponding eigenenergies ϵ can be indexed by a wave vector **k** and a band index n. The wave vector can be considered to lie in a unit cell of the reciprocal space—for instance in the first Brillouin zone (see Figure 1) and the band index n is a natural number. The eigenfunction can without loss of generality be written as a plane wave expansion

$$\psi_{\mathbf{k},n}(\mathbf{r}) = \sum_{\mathbf{G}} c_{\mathbf{k}-\mathbf{G},n}\, e^{i(\mathbf{k}-\mathbf{G})\cdot\mathbf{r}} \tag{21}$$

where the summation runs over all reciprocal lattice vectors **G**. See e.g. ref 10, p 138. The coefficients $c_{\mathbf{k}-\mathbf{G},n}$ and the eigenenergies $\epsilon_{\mathbf{k},n}$ are determined by the infinite set of coupled equations

$$(\epsilon^0_{\mathbf{k}-\mathbf{G}} - \epsilon_{\mathbf{k},n})\, c_{\mathbf{k}-\mathbf{G},n} + \sum_{\mathbf{G}'} U_{\mathbf{G}'-\mathbf{G}}\, c_{\mathbf{k}-\mathbf{G}',n} = 0 \tag{22}$$

where the free electron energy is defined by $\epsilon^0_{\mathbf{k}} = (\hbar^2\mathbf{k}^2)/2m_e$.

We now assume that for a given vector **k** there is m reciprocal vectors $\mathbf{G}_1, \mathbf{G}_2, ..., \mathbf{G}_m$ such that the free energies $\epsilon^0_{\mathbf{k}-\mathbf{G}_1}, \epsilon^0_{\mathbf{k}-\mathbf{G}_2}, ..., \epsilon^0_{\mathbf{k}-\mathbf{G}_m}$ are within the order V of the Fourier coefficients in (20) of each other, but far apart from the other $\epsilon^0_{\mathbf{k}-\mathbf{G}}$ on the scale of V

$$|\epsilon^0_{\mathbf{k}-\mathbf{G}} - \epsilon^0_{\mathbf{k}-\mathbf{G}i}| \gg V, \quad i = 1, ..., m; \quad \mathbf{G} \neq \mathbf{G}_1, ..., \mathbf{G}_m \tag{23}$$

In ref 10, p 155, it is shown that in this case (22) can to leading order in V be replaced by the far simpler set of m coupled equations

$$(\epsilon^0_{\mathbf{k}-\mathbf{G}j} - \epsilon_{\mathbf{k},n})\, c_{\mathbf{k}-\mathbf{G}j,n} + \sum_{i=1}^{m} U_{\mathbf{G}_i-\mathbf{G}_j} c_{\mathbf{k}-\mathbf{G}_i,n} = 0 \tag{24}$$

The eigenfunction with eigenenergy $\epsilon_{\mathbf{k},n}$ is then approximated

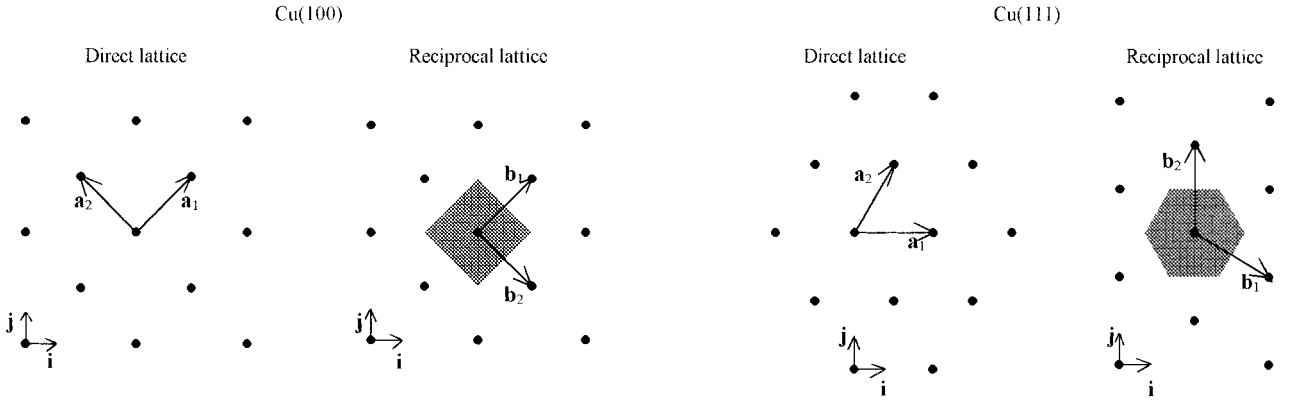

Figure 1. Direct and the reciprocal lattice of the Cu(100) and the Cu(111) surface. The black dots symbolizes the atoms of the lattice for the direct and the reciprocal lattices. $\mathbf{a}_1$, $\mathbf{a}_2$ and $\mathbf{b}_1$, $\mathbf{b}_2$ are the basis vectors of the direct and reciprocal lattice, respectively. The shaded areas show the Brillouin zones.

by the finite sum

$$\psi_{\mathbf{k},n}(\mathbf{r}) = \sum_{i=1}^{m} c_{\mathbf{k}-\mathbf{G}_i,n} e^{i(\mathbf{k}-\mathbf{G}_i)\cdot\mathbf{r}} \tag{25}$$

We choose U_0 in Table 1 so small that this week coupling limit is fulfilled. Physically this corresponds to the fact that the conducting electrons of copper in many ways behave like free electrons.

4.2.1. 1D-Model. In accordance with the former investigation[4] we take the interval [0, G_1 [where $G_1 = 2\pi/d_{1d}$ as the unit cell of the reciprocal space and invoke a two-band model by using the free-electron energies ϵ_k^0 and $\epsilon_{k-G_1}^0$ in (24). Equation 24 then determines the two lowest energy bands and the corresponding normalized eigenvectors. The expressions for the energy bands are then ($\epsilon_{k,1} = \epsilon_k^+$, $\epsilon_{k,2} = \epsilon_k^-$)

$$\epsilon_k^+ = \frac{1}{2}[\epsilon_{k-G_1}^0 + \epsilon_k^0 + \sqrt{(\epsilon_{k-G_1}^0 - \epsilon_k^0)^2 + 4U_0}] \tag{26}$$

$$\epsilon_k^- = \frac{\epsilon_k^0 \epsilon_{k-G_1}^0 - U_0^2}{\epsilon_k^+} \tag{27}$$

The coefficients of the corresponding normalized eigenvectors are ($c_{k,1} = c_k^+$, $c_{k-G_1,1} = c_{k-G_1}^+$, $c_{k,2} = c_k^-$, $c_{k-G_1,2} = c_{k-G_1}^-$) with

$$c_k^{\pm} = \pm \frac{U_0}{\sqrt{U_0^2 + (\epsilon_k^0 - \epsilon_k^{\pm})^2}} \tag{28}$$

$$c_{k-G1}^{\pm} = \pm\sqrt{1 - c_k^{\pm 2}}$$

4.2.2. 2D-Model. We take the first Brillouin zone as the unit cell in the reciprocal space.

A good approximation to the bandstructure for the Cu(100) surface is obtained by invoking a five-band model by using the free electron energies $\epsilon_{\mathbf{k}}^0$, $\epsilon_{\mathbf{k}-\mathbf{b}_1}^0$, $\epsilon_{\mathbf{k}+\mathbf{b}_1}^0$, $\epsilon_{\mathbf{k}+\mathbf{b}_2}^0$, $\epsilon_{\mathbf{k}+\mathbf{b}_2}^0$ in (24). It is exactly those free electron energies which are nearly equal for **k** in the neighborhood of the center of the Brillouin zone. Equation 24 then reduces to

$$\begin{pmatrix} \epsilon_{\mathbf{k}-\mathbf{b}_1}^0 - \epsilon_{\mathbf{k},n} & 0 & U_0 & 0 & 0 \\ 0 & \epsilon_{\mathbf{k}-\mathbf{b}_2}^0 - \epsilon_{\mathbf{k},n} & U_0 & 0 & 0 \\ U_0 & U_0 & \epsilon_{\mathbf{k}}^0 - \epsilon_{\mathbf{k},n} & U_0 & U_0 \\ 0 & 0 & U_0 & \epsilon_{\mathbf{k}+\mathbf{b}_2}^0 - \epsilon_{\mathbf{k},n} & 0 \\ 0 & 0 & U_0 & 0 & \epsilon_{\mathbf{k}+\mathbf{b}_1}^0 - \epsilon_{\mathbf{k},n} \end{pmatrix} \times \begin{pmatrix} c_{\mathbf{k}-\mathbf{b}_1,n} \\ c_{\mathbf{k}-\mathbf{b}_2,n} \\ c_{\mathbf{k},n} \\ c_{\mathbf{k}+\mathbf{b}_2,n} \\ c_{\mathbf{k}+\mathbf{b}_1,n} \end{pmatrix} = \begin{pmatrix} 0 \\ 0 \\ 0 \\ 0 \\ 0 \end{pmatrix} \tag{29}$$

This system of coupled linear equations is solved numerically. The two lowest energy bands of the solution are shown in Figure 2.

For the Cu(111) surface it is actually nessecary to use a seven-band model because both $\epsilon_{\mathbf{k}}^0$, $\epsilon_{\mathbf{k}-\mathbf{b}_1}^0$, $\epsilon_{\mathbf{k}+\mathbf{b}_1}^0$, $\epsilon_{\mathbf{k}-\mathbf{b}_2}^0$, $\epsilon_{\mathbf{k}+\mathbf{b}_2}^0$, $\epsilon_{\mathbf{k}-(\mathbf{b}_1+\mathbf{b}_2)}^0$ and $\epsilon_{\mathbf{k}+(\mathbf{b}_1+\mathbf{b}_2)}^0$ are nearly equal when **k** is close to the center of the first Brillouin zone. Equation 24 then reduces to a set of seven coupled linear equations instead of the five coupled linear equations given in (29). This set of seven coupled linear equations is solved numerically. The two lowest energy bands of the solution are shown in Figure 3. To reduce the computation time we have as well used a five-band model for the Cu(111) surface by using (24) with the free electron-energies $\epsilon_{\mathbf{k}}^0$, $\epsilon_{\mathbf{k}-\mathbf{b}_1}^0$, $\epsilon_{\mathbf{k}+\mathbf{b}_1}^0$, $\epsilon_{\mathbf{k}-\mathbf{b}_2}^0$, $\epsilon_{\mathbf{k}+\mathbf{b}_2}^0$. The two lowest energy bands of the solution are shown in Figure 4.

5. The Interaction Potential

The last requirement in order to calculate the effective potential $V_{\text{eff}}^{\text{elho}}$ is an expression for the matrixelements U_{ij}. As in the previous work we imagine that the nonadiabatic electronic excitations is induced by the interaction of the excess charge on the molecule and the electrons in the metal. We assume that the interaction can be described by a screened Coulomb potential U_C, i.e.

$$U_C = \sum_{i\in\{1,2\}} -\frac{e^2\delta_i(z_i,r)}{X_i} e^{-k_c X_i} \tag{30}$$

where X_i is the distance between the electron and the excess charge $e\delta_i(z_i,r)$ on the atom number i of the molecule, z_i is the distance of the atom number i from the surface, r is the bonding length of the molecule, and k_c is the screening wavenumber. We consider the screening wavenumber to be a parameter and for simplicity use the parameter a defined by

$$k_c = a k_F \tag{31}$$

where k_F is the Fermi vector. As mentioned below the Fermi−Thomas model give a screening proportional to $(k_F)^{1/2}$. We have however chosen to parameterize it by the above expression such that the magnitude of a is directly the screening length (in Å).

The excess charge is as described in ref 7 determined by an analytic fit to the ab initio data of Madhaven and Whitten.[11]

The calculation of the matrixelements $U_{ij} = \langle\psi_{\mathbf{k},n}|U_C|\psi_{\mathbf{k}',n'}\rangle$ in the expression for the effective potential is faciliated by making a Fourier expansion of (30). In the case where the electrons are restricted to move in one dimension we have:

$$U_C = \sum_{j\in\{1,2\}} \frac{e^2\delta(z_j,r)}{d_{1D}\pi} \sum_{m=-\infty}^{m=\infty} e^{im(x/d_{1D})} K_0\left(z_j\sqrt{\left(\frac{m}{d_{1D}}\right)^2 + k_c^2}\right) \tag{32}$$

where K_0 is a Bessel function and x is the position of the electron. This expression is used in the 1D-model. In the case where the electrons are allowed to move in two dimensions (x, y) the result[3] is

$$U_C = \sum_{j\in\{1,2\}} \frac{e^2\delta(z_j,r)}{2\pi\, d_{2D}} \sum_{m=-\infty}^{m=\infty}\sum_{h=-\infty}^{h=\infty} e^{im(x/d_{2D})+ih(y/d_{2D})} \times \frac{1}{\sqrt{h^2 + m^2 + (d_{2D}k_c)^2}} e^{-z_j\{k_c^2 + (h/d_{2D})^2 + (m/d_{2D})^2\}^{1/2}} \tag{33}$$

This expression is then used in the 2D-model. Because both the interaction potential U_C and the one-electron wave functions are written as a plane wave expansion it is now possible to calculate the matrix elements by using the condition: $\langle e^{imx}|e^{inx}\rangle = 2\pi\delta_{n,m}$, where $\delta_{n,m}$ is a Kronecker δ-function.

5.1. 1D-model. In the 1D-model we use a two-band model for the bandstructure. The expression for the one-electon wave function is then

$$\psi_{k,n} = c_{k-G_1}\, e^{i(k-G_1)x} + c_k\, e^{ik\cdot x}$$

and therefore

$$U_{(k,n),(k',n')} = \sum_{j\in\{1,2\}} \frac{2e^2\delta(z_j,r)}{d_{1D}} K_0\left(z_j\sqrt{\left(\frac{m}{d_{1D}}\right)^2 + k_c^2}\right) \times$$

$$\begin{Bmatrix} c_{k,n}c_{k',n'} + c_{k-G_1,n}c_{k'-G_1,n'} & \text{if } k' = k - (m/d_{1D}) \\ c_{k-G_1,n}c_{k',n'} & \text{if } k' = k - G_1 - (m/d_{1D}) \\ c_{k,n}c_{k'-G_1,n'} & \text{if } k' = k + G_1 - (m/d_{1D}) \end{Bmatrix} \quad (34)$$

where $G_1 = 2\pi/d_{1D}$ and m is an integer. Please note that for each state $i = (k, n)$ the states $i' = (k', n')$ for which $U_{i,i'}$ is different from 0 are characterized by only three possible values of k'. We therefore say that we have three "selection rules".

5.2. 2D-Model. In the cases where we use a five-band model for the band structure in the 2D-model (25) reduces to

$$\psi_{\mathbf{k},n} = c_{\mathbf{k}-\mathbf{b}_1,n}\, e^{i(\mathbf{k}-\mathbf{b}_1)\cdot\mathbf{r}} + c_{\mathbf{k}-\mathbf{b}_2,n}\, e^{i(\mathbf{k}-\mathbf{b}_2)\cdot\mathbf{r}} + c_{\mathbf{k},n}\, e^{i\mathbf{k}\cdot\mathbf{r}} + c_{\mathbf{k}+\mathbf{b}_1,n}\, e^{i(\mathbf{k}+\mathbf{b}_1)\cdot\mathbf{r}} + c_{\mathbf{k}+\mathbf{b}_2,n}\, e^{i(\mathbf{k}+\mathbf{b}_2)\cdot\mathbf{r}}$$

By using this expression we get

$$U_{(k,n),(k',n')} = \sum_{j\in\{1,2\}} \frac{e^2\delta(z_j,r)}{2\pi\, d_{2D}} \sum_{m=-\infty}^{m=\infty} \sum_{h=-\infty}^{h=\infty} \frac{1}{\sqrt{h^2 + m^2 + (d_{2D}k_c)^2}} \times e^{-z_j\{k_c^2 + (h/d_{2D})^2 + (m/d_{2D})^2\}^{1/2}} \times \langle\psi_{\mathbf{k},n}|e^{im(x/d_{2D})+ih(y/d_{2D})}|\psi_{\mathbf{k}',n'}\rangle$$

with $\langle\psi_{\mathbf{k},n}\,|e^{im(x/d_{2D})+ih(y/d_{2D})}|\psi_{\mathbf{k}',n'}\rangle$ given by

$$\langle\psi_{\mathbf{k},n}\,|e^{im(x/d_{2D})+ih(y/d_{2D})}|\psi_{\mathbf{k}',n'}\rangle =$$

$$2\pi \begin{cases} \left.\begin{matrix} c_{\mathbf{k}-\mathbf{b}_1,n}c_{\mathbf{k}'-\mathbf{b}_1,n'} + \\ c_{\mathbf{k}-\mathbf{b}_2,n}c_{\mathbf{k}'-\mathbf{b}_2,n'} + c_{\mathbf{k},n}c_{\mathbf{k}',n'} + \\ c_{\mathbf{k}+\mathbf{b}_2,n}c_{\mathbf{k}'+\mathbf{b}_2,n'} + c_{\mathbf{k}+\mathbf{b}_1,n}c_{\mathbf{k}'+\mathbf{b}_1,n'} \end{matrix}\right\} \text{if } \mathbf{k}' = \mathbf{k} - (m/d_{2D}, h/d_{2D}) \\ c_{\mathbf{k}-\mathbf{b}_2,n}c_{\mathbf{k}',n'} + c_{\mathbf{k},n}c_{\mathbf{k}'+\mathbf{b}_2,n'} \text{ if } \mathbf{k}' = \mathbf{k} - (m/d_{2D}, h/d_{2D}) - \mathbf{b}_2 \\ c_{\mathbf{k}+\mathbf{b}_2,n}c_{\mathbf{k}',n'} + c_{\mathbf{k},n}c_{\mathbf{k}'-\mathbf{b}_2,n'} \text{ if } \mathbf{k}' = \mathbf{k} - (m/d_{2D}, h/d_{2D}) + \mathbf{b}_2 \\ c_{\mathbf{k}-\mathbf{b}_1,n}c_{\mathbf{k}',n'} + c_{\mathbf{k},n}c_{\mathbf{k}'+\mathbf{b}_1,n'} \text{ if } \mathbf{k}' = \mathbf{k} - (m/d_{2D}, h/d_{2D}) - \mathbf{b}_1 \\ c_{\mathbf{k}+\mathbf{b}_1,n}c_{\mathbf{k}',n'} + c_{\mathbf{k},n}c_{\mathbf{k}'-\mathbf{b}_1,n'} \text{ if } \mathbf{k}' = \mathbf{k} - (m/d_{2D}, h/d_{2D}) + \mathbf{b}_1 \\ c_{\mathbf{k}-\mathbf{b}_2,n}c_{\mathbf{k}'+\mathbf{b}_2,n'} \text{ if } \mathbf{k}' = \mathbf{k} - (m/d_{2D}, h/d_{2D}) - 2\mathbf{b}_2 \\ c_{\mathbf{k}+\mathbf{b}_2,n}c_{\mathbf{k}'-\mathbf{b}_2,n'} \text{ if } \mathbf{k}' = \mathbf{k} - (m/d_{2D}, h/d_{2D}) + 2\mathbf{b}_2 \\ c_{\mathbf{k}-\mathbf{b}_2,n}c_{\mathbf{k}'-\mathbf{b}_1,n'} + c_{\mathbf{k}+\mathbf{b}_1,n'}c_{\mathbf{k}'+\mathbf{b}_2,n'} \text{ if } \mathbf{k}' = \mathbf{k} - (m/d_{2D}, h/d_{2D}) - \mathbf{b}_2 + \mathbf{b}_1 \\ c_{\mathbf{k}-\mathbf{b}_2,n}c_{\mathbf{k}'+\mathbf{b}_1,n'} + c_{\mathbf{k}-\mathbf{b}_1,n}c_{\mathbf{k}'+\mathbf{b}_2,n'} \text{ if } \mathbf{k}' = \mathbf{k} - (m/d_{2D}, h/d_{2D}) - \mathbf{b}_2 - \mathbf{b}_1 \\ c_{\mathbf{k}+\mathbf{b}_2,n}c_{\mathbf{k}'-\mathbf{b}_1,n'} + c_{\mathbf{k}+\mathbf{b}_1,n}c_{\mathbf{k}'-\mathbf{b}_2,n'} \text{ if } \mathbf{k}' = \mathbf{k} - (m/d_{2D}, h/d_{2D}) + \mathbf{b}_2 + \mathbf{b}_1 \\ c_{\mathbf{k}+\mathbf{b}_2,n}c_{\mathbf{k}'+\mathbf{b}_1,n'} + c_{\mathbf{k}-\mathbf{b}_1,n}c_{\mathbf{k}'-\mathbf{b}_2,n'} \text{ if } \mathbf{k}' = \mathbf{k} - (m/d_{2D}, h/d_{2D}) + \mathbf{b}_2 - \mathbf{b}_1 \\ c_{\mathbf{k}-\mathbf{b}_1,n}c_{\mathbf{k}'+\mathbf{b}_1,n'} \text{ if } \mathbf{k}' = \mathbf{k} - (m/d_{2D}, h/d_{2D}) - 2\mathbf{b}_1 \\ c_{\mathbf{k}+\mathbf{b}_1,n}c_{\mathbf{k}'-\mathbf{b}_1,n'} \text{ if } \mathbf{k}' = \mathbf{k} - (m/d_{2D}, h/d_{2D}) + 2\mathbf{b}_1 \end{cases} \quad (35)$$

In this case we get 13 "selection rules". As mentioned in 4.2.2 it is most correct to use a seven-band model for the band structure of the Cu(111) surface in the 2D-model. In the seven-band model the expression replacing (35) instead of 13 contains 19 "selection rules". This expression is not given here.

6. The Simulations

In this section we first describe the simulation procedure briefly. Hereafter we give a survey of how the above defined models were tested in the simulations. In the simulations the movement of each atom of the hydrogen molecule was obtained by numerically integrating the classical equations of motions for the diatomic molecule. The simulation was started with the molecule placed with its center of mass (CM) at a distance of 7 Å from the copper surface. At this distance the effective potential is essentially just the Morse potential of the hydrogen molecule. The integration of the equations of motion was done using a predictor−corrector integrator with variable step length and order. The simulation was stopped when one of the following events occurred:

1. More than the initial translational part of the kinetic energy of the molecule was transferred to the phonons. In this case the molecule was considered *adsorped*.

2. The distance between the atoms of the molecule was larger than 2.5 Å. In this case the molecule was considered *dissociated*.

3. The distance, of the center of mass of the molecule, from the surface was larger than the corresponding initial distance. In this case the molecule was considered to be *scattered*.

In real experiments not all of the initial conditions of the molecule can be even approximately controlled. Often those initial conditions involve the aiming point, the orientation of the molecule, and the binding length. Therefore one chooses these conditions at random and finally make an average of the results obtained with different conditions. However the computation time when using the 2D-model was so long that this approach was not possible because it would require the simulation of too many trajectories. Instead we first at random chose 110 sets of those initial values—"the values of the uncontrolled parameters". Those 110 sets were then used in all the simulations.

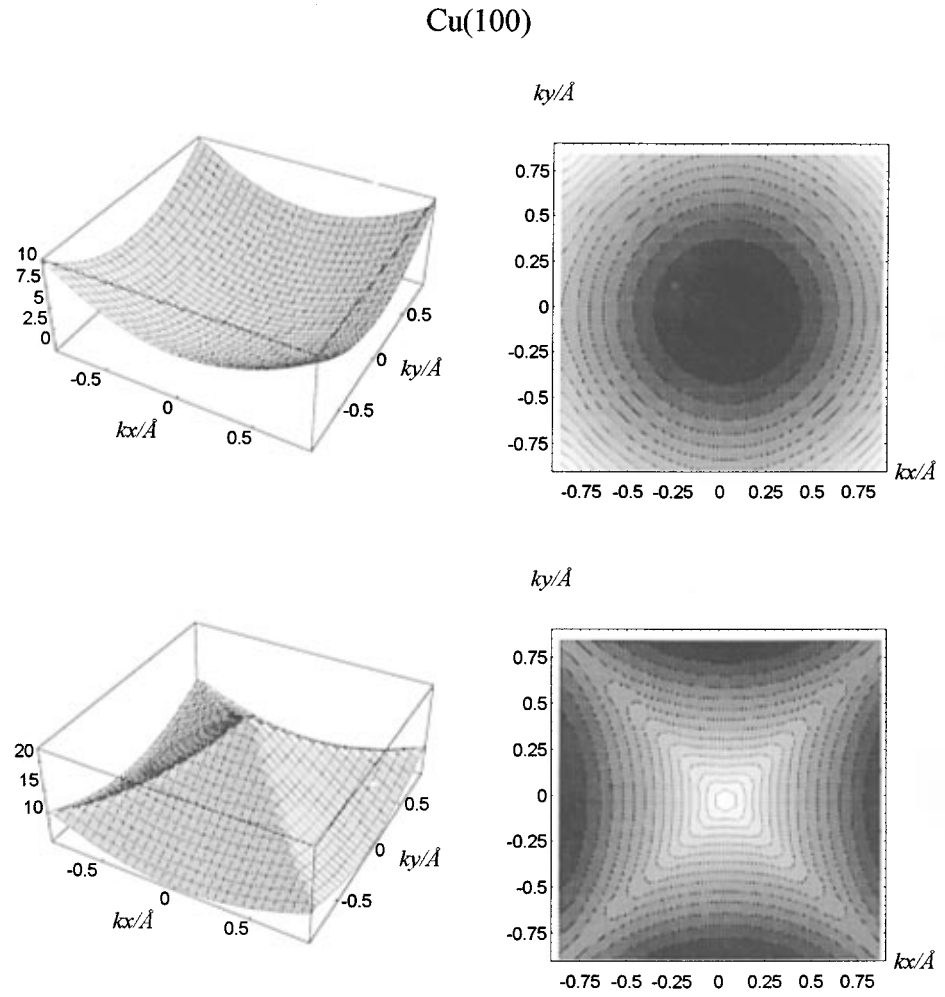

Figure 2. Illustration of the two lowest energy bands of the Cu(100) surface obtained with the five-band model. On the left the 3-D plots of the surfaces are shown and on the right the corresponding contour plots. The unit of the reciprocal wavevectors is $Å^{-1}$ and the energy unit is $\epsilon = 100$ kJ/mol.

TABLE 2: An Overview of the Initial Conditions Used in Testing the Models. $1\ \tau = 10^{-14}$ s

parameter	R_{CM}/Å	P_{CM}/(amu·τ/Å)	J	v	a	T_s/K	θ/deg	ϕ/deg
value	7	1.2, 1.5, 1.7, 2.0	0	0	0.25, 0.5, 1.0	300, 600	0	0, 31.83, 41.41

The rest of the parameters necessary to specify the initial condition are the size of the center of mass momentum, P_{CM}, the direction of the center of mass momentum given by the polar angels θ and ϕ, the internal state of the molecule specified by the quantum numbers J and v, the screening parameter a and the surface temperature T_s. We have used the values of those parameters given in Table 2. Since the same set of random variables are used, we in this way ensure that the observed difference between the results obtained with the three models are due to differences in the models and not to differences in the initial conditions. On the other hand the number of trajectories is sufficient for some important quantities, calculated from the simulations, to be converged.

We now describe which combinations of the 1D-model and the 2D-model with the n-band models of the bandstructure ($n \in \{2, 5, 7\}$) we have used in the simulations.

On the Cu(100) surface we used

1. The 1D-model together with the two-band model for the band structure
2. The 2D-model together with the five-band model for the band structure
3. A model where the electron-hole excitation is neglected. This model is in the following called the "*-elho* model"

On the Cu(111) surface we used

1. The 1D-model together with the two-band model for the band structure
2. The 2D-model together with the five-band model for the band structure
3. The 2D-model together with the seven-band model for the band structure
4. The -elho model

It is not relevant to use the two-band model for the bandstructure together with the 2D-model because the band-structure obtained from the two-band model does not have the symmetry of the atoms of the top layer of the crystal.

The 1D-model is exactly the same for the Cu(100) and Cu-(111) with respect to the treatment of the electron−hole excitation. The effective potential of those two surfaces then only differ in the adiabatic potential and in the effective potential originating from the coupling to the phonons.

In the 2D-model the effective potentials used on the Cu(100) surface and the Cu(111) surface differ as in the 1D-model in the adiabatic potential and the effective potential originating from the coupling to the phonons. But the 2D-model also differ in the effective potential originating from the electron−hole excitation in the metal. Even in the case where a five-band

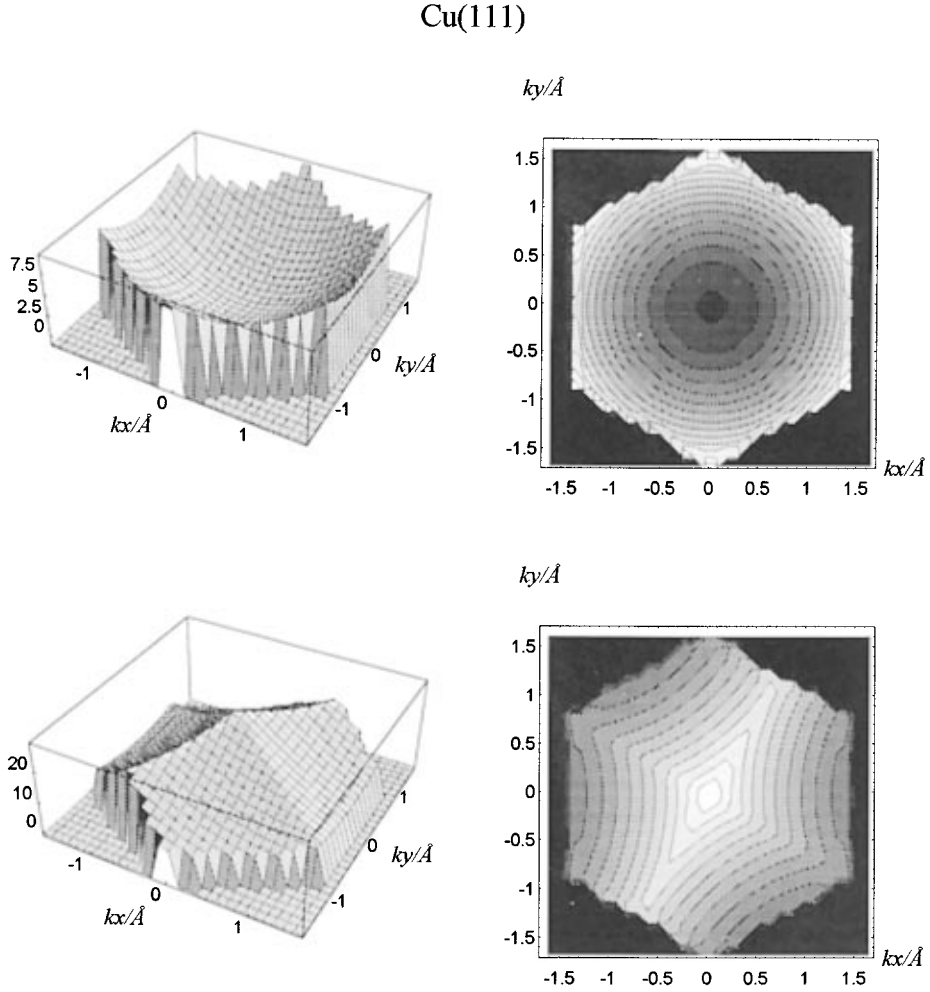

Figure 3. Same as Figure 2 but for the Cu(111) seven-band model.

TABLE 3: The P_{dis} for Cu(100), $T_S = 300$ K, $\theta = \phi = 0$, $J = v = 0$. $1\ \epsilon = 100$ kJ/mol

	−elho model	1D-model			2D-Model (five-bands)		
		$a = 1.00$	$a = 0.50$	$a = 0.25$	$a = 1.00$	$a = 0.50$	$a = 0.25$
$E_i = 0.36\epsilon$	0.00	0.00	0.03	0.19	0.00	0.11	0.30
$E_i = 0.56\epsilon$	0.00	0.01	0.18	0.48	0.01	0.33	0.60
$E_i = 0.72\epsilon$	0.01	0.03	0.26	0.57	0.06	0.42	0.72
$E_i = 1.00\epsilon$	0.11	0.12	0.32	0.62	0.17	0.44	0.74

model is used on both surfaces this potential is different on the two surfaces due to the different basisvectors $\mathbf{b}_1$ and $\mathbf{b}_2$.

When invoking the 2D-model on the Cu(111) surface it is most correct to use the seven-band model for the bandstructure, but as this model as mentioned above is numerically quite complicated we have used the 2D-model together with the five-band model in many of the simulations. We have chosen to report results for various values of the screening parameter ak_F. Application of the Fermi−Thomas model for this parameter gives $(k_F)^{1/2}$. Since k_F is 1.36 Å^{-1} for copper this model corresponds to $a = 1.3$ Å.

7. Results and Discussion

From the results of each series of 110 simulations we have calculated the following quantities: The probability of dissociation (P_{dis}), the probability of adsorption (P_{ads}), the probability of scattering (P_{scat}), the final kinetic (E_{kin}), rotational (E_{rot}), and vibrational energy (E_{vib}). Also the energy transferred to the phonons (E_{int}) and to the electrons of the metal (E_{elho}) are reported.

Below we present some of the results discussing the following three questions:

1. Do the different models give different values of the just mentioned quantities for the same initial conditions?

2. Do the values of those quantities determined by the different models have different functional dependences on the initial conditions?

3. On purely theoretical grounds one must expect that the 2D-model is the most realistic. But will a comparison with experimental results also suggest that it is necessary to use the much more elaborate 2D-model?

7.1. Different Values. The answer to the first question is yes. The effect is most pronounced for the probability of dissociation (P_{dis}) and for the probability of scattering ($P_{scat} = 1 - (P_{ads} + P_{dis})$). The values of P_{dis} determined with three different values of a (in Å) are given as a function of the initial kinetic energy ($E_i = P_{CM}^2/2m$ where m is the mass of the hydrogen molecule) in Table 3 for the Cu(100) surface and in Table 4 for the Cu(111) surface. The values of ($P_{ads} + P_{dis}$) are in the same way given in Table 5 for the Cu(100) surface

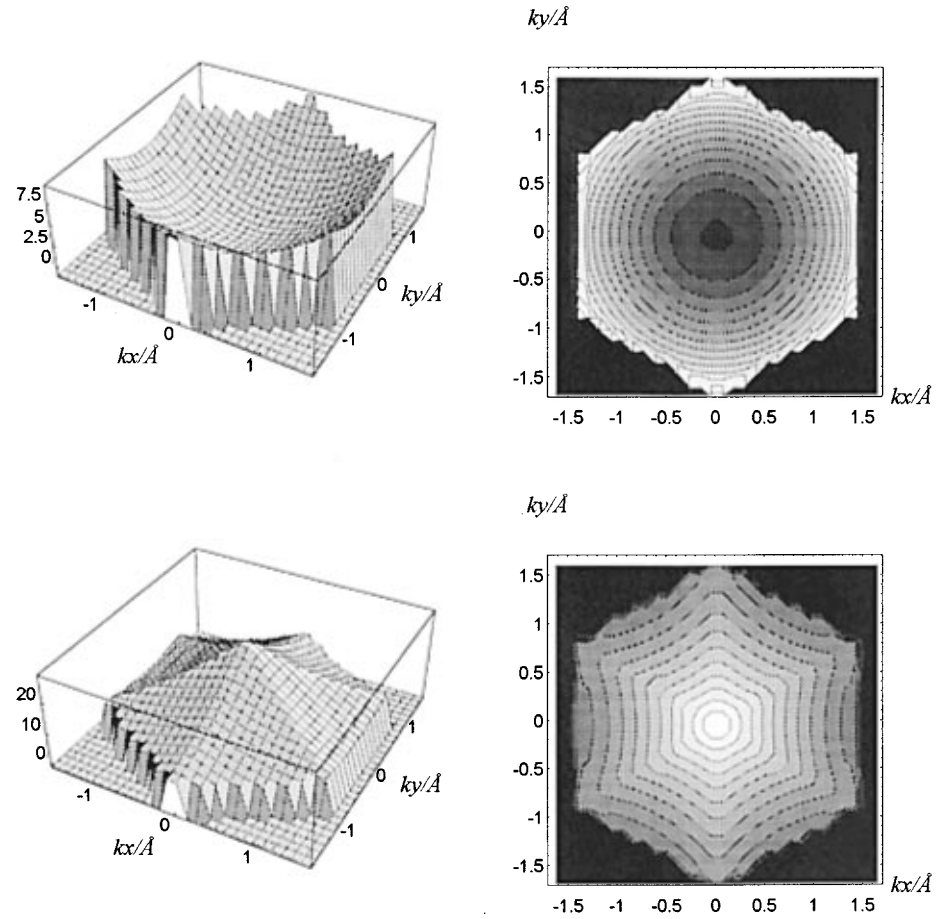

Figure 4. Same as Figure 2 but for the Cu(111) five-band model.

TABLE 4: P_{dis} for Cu(111), $T_s = 300$ K, $\theta = \phi = 0$, $J = v = 0$. $1\ \epsilon = 100$ kJ/mol

		1D-model			2D-model (five-bands)			2D-model (seven bands)
	−elho model	$a = 1.00$	$a = 0.50$	$a = 0.25$	$a = 1.00$	$a = 0.50$	$a = 0.25$	$a = 0.5$
$E_i = 0.36\epsilon$	0.00	0.00	0.00	0.08	0.00	0.23	0.39	0.21
$E_i = 0.56\epsilon$	0.00	0.00	0.05	0.29	0.03	0.46	0.68	0.41
$E_i = 0.72\epsilon$	0.00	0.02	0.16	0.37	0.13	0.54	0.78	0.55
$E_i = 1.00\epsilon$	0.08	0.12	0.24	0.40	0.21	0.63	0.85	0.64

TABLE 5: $P_{dis} + P_{ads}$ for Cu(100), $T_s = 300$ K, $\theta = \phi = 0$, $J = v = 0$. $1\ \epsilon = 100$ kJ/mol

		1D-model			2D-model five-bands)		
	−elho model	$a = 1.00$	$a = 0.50$	$a = 0.25$	$a = 1.00$	$a = 0.50$	$a = 0.25$
$E_i = 0.36\epsilon$	0.36	0.36	0.40	0.42	0.37	0.34	0.45
$E_i = 0.56\epsilon$	0.41	0.44	0.65	0.74	0.45	0.67	0.79
$E_i = 0.72\epsilon$	0.32	0.35	0.57	0.72	0.37	0.66	0.83
$E_i = 1.00\epsilon$	0.24	0.30	0.50	0.73	0.34	0.61	0.83

and in Table 6 for the Cu(111) surface. It is seen that the values of P_{dis} obtained with the −elho model are smaller than the results obtained with the 1D-model which in turn are smaller than the results obtained with the 2D-model. The same relation is seen for ($P_{ads} + P_{dis}$). The absolute difference between the results obtained with the three models depends on the initial conditions, but the conclusion that the values obtained by the 2D-model are the largest and the values obtained by the −elho model are the smallest holds for all the investigated initial conditions.

The mean energy transferred to the phonons (E_{int}) by the scattered molecules also shows some dependence on the model. The results are given in Table 7 for the Cu(100) surface and in Table 8 for the Cu(111) surface. It is seen that in general E_{int} for the Cu(111) surface determined with the -elho model was smaller than E_{int} determined with the two other models. The opposite result was observed on the Cu(100) surface. Here the tendency was that the values determined by the -elho model were the biggest.

In the Tables 10, 11 and 12 the values of P_{dis}, $P_{ads} + P_{dis}$, and E_{int} respectively are given for the Cu(111) surface in the case where the angle of incidence was different from 0. The values are given as functions of the so called normal energy

TABLE 6: $P_{dis} + P_{ads}$ for Cu(111), $T_s = 300$ K, $\theta = \phi = 0$, $J = v = 0$. $1\ \epsilon = 100$ kJ/mol

		1D-model			2D-model (five-bands)			2D-model (seven-bands)
	−elho model	$a = 1.00$	$a = 0.50$	$a = 0.25$	$a = 1.00$	$a = 0.50$	$a = 0.25$	$a = 0.5$
$E_i = 0.36\epsilon$	0.11	0.13	0.29	0.48	0.27	0.59	0.61	0.58
$E_i = 0.56e$	0.02	0.04	0.19	0.38	0.19	0.68	0.85	0.67
$E_i = 0.72\epsilon$	0.04	0.07	0.26	0.46	0.25	0.67	0.90	0.67
$E_i = 1.00e$	0.14	0.16	0.31	0.45	0.29	0.70	0.94	0.70

TABLE 7: E_{int} for Cu(100), $T_s = 300$ K, $\theta = \phi = 0$, $J = v = 0$. $1\ \epsilon = 100$ kJ/mol

		1D-model			2D-model (five-bands)		
	−elho model	$a = 1.00$	$a = 0.50$	$a = 0.25$	$a = 1.00$	$a = 0.50$	$a = 0.25$
$E_i = 0.36\epsilon$	0.044	0.047	0.042	0.038	0.044	0.057	0.039
$E_i = 0.56\epsilon$	0.126	0.128	0.102	0.094	0.136	0.117	0.091
$E_i = 0.72e$	0.167	0.158	0.141	0.132	0.168	0.143	0.124
$E_i = 1.00e$	0.215	0.120	0.169	0.156	0.189	0.176	0.173

TABLE 8: E_{int} for Cu(111), $T_s = 300$ K, $\theta = \phi = 0$, $J = v = 0$. $1\ \epsilon = 100$ kJ/mol

		1D-model			2D-model (five-bands)			2D-model (seven-bands)
	−elho model	$a = 1.00$	$a = 0.50$	$a = 0.25$	$a = 1.00$	$a = 0.50$	$a = 0.25$	$a = 0.5$
$E_i = 0.36\epsilon$	0.066	0.068	0.064	0.051	0.067	0.046	0.048	0.048
$E_i = 0.56\epsilon$	0.099	0.102	0.108	0.112	0.106	0.114	0.146	0.117
$E_i = 0.72\epsilon$	0.117	0.120	0.124	0.128	0.123	0.154	0.156	0.179
$E_i = 1.00\epsilon$	0.150	0.152	0.154	0.177	0.160	0.196	0.164	0.193

TABLE 9: E_{int} for Cu(111), $T_s = 600$ K, $\theta = \phi = 0$, $J = v = 0$. $1\ \epsilon = 100$ kJ/mol

	−elho model	1D-model $a = 0.50$	2D-model (five-bands) $a = 0.50$
$E_i = 0.36\epsilon$	0.063	0.064	0.046
$E_i = 0.56$e	0.098	0.105	0.121
$E_i = 0.72\epsilon$	0.116	0.122	0.151
$E_i = 1.00\epsilon$	0.148	0.152	0.193

TABLE 10: P_{dis} for Cu(111), $T_s = 300$ K, $E_i = 1.0\epsilon$, $J = v = 0$. $1\ \epsilon = 100$ kJ/mol

	−elho model	1D-model $a = 0.50$	2D-model (five-bands) $a = 0.50$
$E_n = 0.56\epsilon$	0.00	0.09	0.35
$E_n = 0.72\epsilon$	0.05	0.22	0.58

TABLE 11: $P_{dis} + P_{ads}$ for Cu(111), $T_S = 300$ K, $E_i = 1.0\epsilon$, $J = v = 0$. $1\ \epsilon = 100$kJ/mol

	−elho model	1D-model $a = 0.50$	2D-model (five-bands) $a = 0.50$
$E_n = 0.56\epsilon$	0.02	0.10	0.41
$E_n = 0.72\epsilon$	0.10	0.30	0.65

TABLE 12: E_{int} for Cu(111), $T_S = 300$ K, $E_i = 1.0\epsilon$, $J = v = 0$. $1\ \epsilon = 100$ kJ/mol

	−elho model	1D-model $a = 0.50$	2D-model (five-bands) $a = 0.50$
$E_n = 0.56\epsilon$	0.087	0.092	0.107
$E_n = 0.72\epsilon$	0.115	0.131	0.163

(E_n) defined by $E_n = E_i \cos^2 \theta$. It is seen that in this case the same conclusions concerning the effect of the different models can be drawn.

We have as well made simulations on the Cu(111) surface with the surface temperature (T_s) increased from 30 to 600 K. Only the values of E_{int} were slightly changed. Those values are given in Table 9. We did not make the corresponding simulations on the Cu(100) surface because the observed changes on the Cu(111) surface were quite small.

We have only used the 2D-model together with the seven-band model in the case where the incidence was normal to the surface and the surface temperature 300 K. The reason for this is that we in this case only saw minor differences between the results obtained with the five-band model and the seven-band model. (Compare the results in columns 7 and 9 in Tables 4, 6, and 8.)

We believe that the general conclusions mentioned above are independent of the choice of "the values of the uncontrolled parameters" because we obtained the same results when dividing each series into two equal parts and making the average from each part separately. For the other quantities investigated, i.e., E_{kin}, E_{rot}, E_{vib}, and E_{elho}, the results obtained were not influenced in quite the same systematic way by the models used. This might be due to the fact that the number of simulations (110) in each series is too small.

7.2. Different Functional Dependencies. Now the second question is addressed. We have investigated whether the models cause the above mentioned quantities to depend in different ways on the following parameters:

1. The initial CM momentum P_{CM}
2. The surface temperature T_s
3. The direction of the initial CM momentum specified by the polar angels θ and ϕ
4. The screening factor a
5. The crystal symmetry

The result was that only the dependence on the crystal orientation was different for the 3 models. This effect was seen both in the values of P_{dis} and in the values of ($P_{dis} + P_{ads}$). From the numbers in the Tables 3 and 4 it is clear that when either the -elho model or the 1D-model is used the value of P_{dis} is larger on the Cu(100) surface than on the Cu(111) surface for the same values of E_i and a. But when the 2D-model is used the values for the Cu(111) surface are larger than the values for the Cu(100) surface. The results in Tables 5 and 6 show

that the same conclusion holds for ($P_{dis} + P_{ads}$) for $a = 0.50$ and $a = 0.25$ at the higher energies.

7.3. Experimental Results. Now the third and last question is discussed. The comparison with experimental results is complicated by the fact that in order to reduce computation time the treatment is simplified in some respects:

(1) The motion of the molecule is treated quasi-classically. This implies that the molecule cannot pass the barrier of dissociation if its kinetic energy is less than the dissociation barrier. It also results in that the zero-point vibrational energy is not conserved properly during the simulations. This effect is pronounced because the initial condition $v = 0$ is used in all simulations. Those two effects will influence the results in different ways. The first will tend to reduce the dissociation probability, while the other will tend to increase it. But it is not possible to know wether the two effects balance each other.

(2) The diabatic coupling between the adiabatic potential surfaces is neglected and only the lowest adiabatic potential surface is used.

(3) The motion of each hydrogen molecule is only followed in a very short real time compared with that of a real experiment. This makes it hard to decide whether the experimentally determined dissociation probabilities should be compared to P_{ads}, P_{dis}, or perhaps their sum.

Because of these limitations of the model we do not expect the results to fit the experiments quantitatively. But we find it reasonable to believe that the change in the results caused by a change in the initial conditions will resemble the change of the experimental results corresponding to a change in the experimental conditions. Above we have mentioned that P_{dis} and to a certain extent ($P_{dis} + P_{ads}$) show a different dependence on the surface structure for the different models investigated. In ref 12 investigations of the sticking probability is reported for both Cu(100) and Cu(111) as a function of E_{kin} for E_{kin} in the interval [0.2ϵ,0.4ϵ]. The result is that for all the experimental conditions investigated the sticking probability is larger on the Cu(111) surface than on the Cu(100) surface. This is in accordance with the results obtained with the 2D-model both in the case where the five-band and where the seven-band model is used for the bandstructure of the Cu(111) surface if the sticking probability is interpreted as P_{dis}. But the results of the simulations with the -elho model or the 1D-model are in contrast to the results of ref 12 if P_{dis} is used for the sticking probability. If the sticking probability is interpreted as ($P_{dis} + P_{ads}$) the same conclusion holds for $a = 0.25$ and $a = 0.50$ for the larger kinetic energies.

8. Conclusion

We have extended an existing model for the coupling of the hydrogen molecule to the conduction electrons of the copper metal. The new model includes the symmetry of the crystal in the bandstructure of the electrons of the metal. Therefore the corresponding effective potential is different for the Cu(100) and the Cu(111) surface. We have performed simulations with the extended model to see wether the change does influence the results. We have only made series of 110 simulations but this number is big enough for seeing an influence of the model on the "sticking probability". We did not expect the results to be in complete agreement with experimental results because the model is simplified in some important respects. But we saw that when using the extended model the functional dependency of the "sticking probability" on the surface symmetry is in accordance with experiments. In the case where we used the models which did not include the symmetry of the crystal in the band structure the functional dependency of the "sticking probability" on the surface symmetry was not consistent with the experimental results. We therefore conclude that the extension of the model is important.

Acknowledgment. This research is supported by the Danish Natural Science Research Council.

References and Notes

(1) See e.g.: White, J. A.; Bird, D. M. *Chem. Phys. Lett.* **1993**, *213*, 422. White, J.A.; Bird, J. M.; Payne M.; Stich, I. *Phys. Rev. Lett.* **1994**, *93*, 1404. Hammer, B.; Scheffler, M.; Jacobsen, K. W.; Nørskov, J. K. *Phys. Rev. Lett.* **1994**, *73*, 1400. Wiesnekker, G.; Kroes, G. J.; Baerends E. J.; Mowrey, R. C. *J. Chem. Phys.* **1995**, *102*, 3873.

(2) Hansen, B. F.; Billing, G. D. *Surf. Sci. Lett.* **1997**, *373*, 333.

(3) Billing, G. D. *J. Phys. Chem.* **1995**, *99*, 15378.

(4) Billing, G. D. *Chem. Phys.* **1987**, *116*, 269.

(5) Billing, G. D. *Chem. Phys.* **1982**, *70*, 223.

(6) Billing, G. D. *Chem. Phys.* **1983**, *74*, 143.

(7) Billing, G. D. *Comp. Phys. Rep.* **1990**, *12*, 383.

(8) White, J. A.; Bird, D. M. *Chem. Phys. Lett.* **1993**, *213*, 422.

(9) Truong, T. N.; Truhlar, D. G.; Garrett, B. C. *J. Chem. Phys.* **1989**, *93*, 8227.

(10) Ashcroft, N. W.; Mermin, N. D. *Solid State Physics*; Samdes College Publishers, 1976.

(11) Madhaven, P.; Whitten, J. L. *J. Chem. Phys.* **1982**, *77*, 2673.

(12) Angel, G.; Winkler, A.; Rendulic, K. D. *Surf. Sci.* **1989**, *220*, 1.